Title

Electrocatalytic Methane Functionalization with d0 Early Transition Metals Under Ambient Conditions

Journal

Angewandte Chemie International Edition, 60(51)

ISSN

1433-7851

Authors

Deng, Jiao
Lin, Sheng-Chih
Fuller, Jack T
et al.

Publication Date

2021-12-13

DOI

10.1002/anie.202107720

Peer reviewed

Electrocatalytic Methane Functionalization with d^0 Early Transition Metals Under Ambient Conditions

Jiao Deng,[a]‡ Sheng-Chih Lin,[b]‡ Jack T. Fuller, III,[a]‡ Borna Zandkarimi,[a] Hao-Ming Chen,[b]* Anastassia N. Alexandrova,[a,c]* Chong Liu[a]*

[a] Dr. J. Deng, J. T. Fuller, III, B. Zandkarimi, Prof. Dr. A. N. Alexandrova, Prof. Dr. C. Liu
Department of Chemistry and Biochemistry
University of California, Los Angeles
Los Angeles, California 90095, United States
E-mail: ana@chem.ucla.edu; chongliu@chem.ucla.edu

[b] S. C. Lin, Prof. Dr. H. M. Chen
Department of Chemistry
National Taiwan University
Taipei 10617, Taiwan
E-mail: haomingchen@ntu.edu.tw

[c] Prof. Dr. A. N. Alexandrova
California NanoSystems Institute
Los Angeles, California 90095, United States

‡ These authors contributed equally to this work

Supporting information for this article is given via a link at the end of the document.

Abstract: The undesirable loss of methane (CH_4) at remote locations welcomes approaches that ambiently functionalize CH_4 on-site without intense infrastructure investment. Recently, we found that electrochemical oxidation of vanadium(V)-oxo with bisulfate ligand leads to CH_4 activation at ambient conditions. The key question is whether such an observation is a one-off coincidence or a general strategy for electrocatalyst design. Here, a general scheme of electrocatalytic CH_4 activation with d^0 early transition metals is established. The pre-catalysts' molecular structure, electrocatalytic kinetics, and mechanism were detailed for titanium (IV), vanadium (V), and chromium (VI) species as model systems. After a turnover-limiting one-electron electrochemical oxidation, the yielded ligand-centered cation radicals activate CH_4 with low activation energy and high selectivity. The reactivities are universal among early transition metals from Period 4 to 6, and the reactivities trend for different early transition metals correlate with their d orbital energies across periodic table. Our results offer new chemical insights towards developing advanced ambient electrocatalysts of natural gas.

Introduction

Methane (CH_4), the primary constituent of natural gas with wide geological distribution, could have been better utilized especially at remote locations where the long-range transport of gaseous resources is uneconomical and flaring or direct emission of CH_4 into the atmosphere are practiced.[1] An on-site conversion of natural gas including CH_4 into liquid fuels or value-added chemicals with minimal reliance on a centralized chemical infrastructure offers a viable solution to mitigate such an issue.[1b] Yet current industrial process of CH_4 utilization is not amenable to the desired minimal reliance on infrastructure, because it undergoes a two-step indirect route of transformation that includes steam reforming of CH_4 into syngas (CO/H_2) at high pressure (30 bar) and elevated temperature (650 °C).[2] Similarly, solution-phase reactions of CH_4 functionalization usually demand high pressure and/or elevated temperature,[3] as the reactivities of catalytic intermediates are insufficient at ambient conditions to overcome the high kinetic barrier of C-H activation in CH_4. An alternative approach is welcomed for direct CH_4 functionalization under mild and, if possible, ambient conditions.

Electrochemical catalysis offers an opportunity of activating strong covalent bonds in small molecular substrates at ambient conditions, evident recently in the broad demonstrations of electrocatalytic conversion of carbon dioxide (CO_2) and even dinitrogen (N_2).[4] We envision that an ambient CH_4 functionalization into commodity chemicals can be achieved with electrochemical catalysis, because electrochemical charge transfer is capable of generating highly CH_4-reactive intermediates otherwise inaccessible ambiently.[5] Enlightening works have been reported for electrocatalysis mediated by Pt and Pd-based species at 70 ~ 140 ºC and 34 ~ 47 bar CH_4,[6] taking advantage of the molecular Pt and Pd catalysts that activate CH_4 via electrophilic activation.[3d, 3m] In line with our stated vision, we are particularly interested in exploring and designing new electrocatalytic systems with reaction mechanisms that have few correspondences in solution catalysis and are unique to electrochemistry. One of our recent contributions is our discovery that electrochemical oxidation of a d^0 vanadium(V)-oxo dimer in 98% H_2SO_4 yields a cation radical on the bound bisulfate ligand that selectively activates CH_4 at ambient conditions.[7] Benefiting from its uncommon mechanism with a turnover-limiting one-electron removal prior to the step of C-H activation, this homogenous molecular electrocatalyst converts CH_4 into methyl bisulfate (CH_3OSO_3H) at room temperature, with a high Faradaic efficiency (up to 84.5% at 3 bar CH_4), a low apparent

activation energy (10.8 kcal/mol), and a turnover number beyond 45,000 with a duration up to 72 hours. Despite such favorable properties, the question remains: is this discovery a mere one-off coincidence or representing a whole class of homogenous electrocatalysis based on transition metals? Understanding the reaction mechanism and general applicability of those electrochemistry-enabled catalysis will offer a rational design principle and

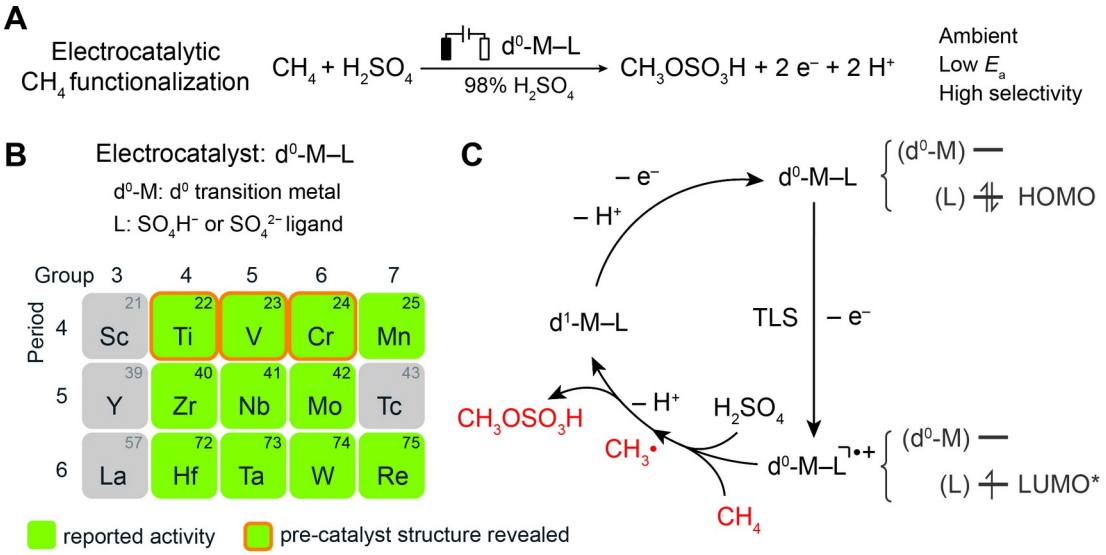

Figure 1. (A) The electrocatalytic half-reaction of CH_4 functionalization catalyzed by d^0 early transition metal pre-catalyst (d^0-M–L) in 98% H_2SO_4. E_a, apparent activation energy. (B) The reported d^0-M–L pre-catalysts over the periodic table (green). More detailed study has been devoted to Ti^{IV}, V^V, and Cr^{VI} (highlighted in red). (C) The proposed electrocatalytic cycle of CH_4 activation with the frontier orbitals for d^0-M–L and the electrochemically generated ligand-centered cation radicals d^0-M–$L^{\bullet+}$. TLS, turnover-limiting step; HOMO, highest occupied molecular orbital; LUMO*, lowest unoccupied molecular orbital when considering spin-orbital coupling, equivalent to singly occupied molecular orbital (SOMO) in restricted formalism.

maximize the stated benefit of electrochemistry that generates highly reactive intermediate towards ambient CH_4 functionalization, which may guide an economical technology development of CH_4 utilization by considering available transition metal storage in different countries and regions.

In this work, we report a class of molecular electrocatalysts for CH_4 activation that covers the majority of d^0 early transition metals, generally noted as d^0-M−L (M, metal; L, ligand), from Period 4 to Period 6 in the periodic table (Figure 1). A systematic study revealed that titanium (IV) (Ti^{IV}), vanadium (V) (V^V), and chromium (VI) (Cr^{VI}) model pre-catalysts in 98% H_2SO_4 share similar molecular binding motifs, exhibit similar electrocatalytic kinetics (~120 mV/dec Tafel slope) and apparent activation energies (12.9 ~ 17.7 kcal/mol), as well as are proposed to follow the same electrocatalytic mechanism. After a turnover-limiting one-electron electrochemical oxidation, the yielded cation radicals centered on the ligand's O atom (d^0-M−$L^{\bullet+}$) initiate ambient CH_4 functionalization with low activation energy and high electrochemical selectivity (Figure 1C). An expanded survey across all of the soluble and isotopically stable early transition metals in 98% H_2SO_4 indicates that d^0 early transition metals are in general all electrocatalytic towards CH_4 at ambient conditions. Moreover, the reactivity trend is correlated with metals d orbital's energy and its overlap with the O 2p orbital in the ligand. These findings led us to establish working hypotheses and design principles of electrochemical CH_4 functionalization at mild conditions for the better utilization of natural gas resources in the future.

Results and Discussion

We sought to investigate the general applicability of d^0 early transition metals (d^0-M−L) for electrocatalytic CH_4 activation inspired by our prior serendipitous discovery[7] and the first expanded set of tested elements were the Period 4 early transition metals: Ti^{IV}, V^V, and Cr^{VI}. We were unable to test the reactivity of Sc^{III} because there is not a simple, commercially available Sc^{III} compound soluble in 98% H_2SO_4. Ti^{IV}, V^V, and Cr^{VI} molecular pre-catalysts were prepared by dissolving titanyl sulfate ($TiOSO_4$), vanadium pentoxide (V_2O_5), and potassium chromate (K_2CrO_4) in 98% H_2SO_4, respectively (Experiments and Methods in SI). Cyclic voltammograms for 10 mM Ti^{IV}, V^V, and Cr^{VI} in 98% H_2SO_4 were measured under 1-bar N_2 and CH_4 at 25 °C on the working electrodes of fluorine-doped tin oxide (FTO) (Figures 2A and S1). Under 1-bar N_2, the redox couples of $Ti^{III/IV}$, $V^{IV/V}$, and $Cr^{III/VI}$ (Figure S1) were assigned to the observed electrochemical potentials of cathodic and anodic peaks (E_{red} and E_{ox}, respectively).[8] E_{red} = −0.30 V, 0.33 V and 0.21 V and E_{ox} = 0.20 V, 1.25 V, and 2.05 V vs. Hg_2SO_4/Hg for $Ti^{III/IV}$, $V^{IV/V}$, and $Cr^{III/VI}$, respectively. The broad redox peaks shown in cyclic voltammograms, specially for Cr, suggest sluggish kinetics for the charge transfer on the metal centers.[8c, 9] When the gas environment was switched from N_2 to CH_4 of ambient pressure, the redox peaks of $Ti^{III/IV}$, $V^{IV/V}$, and $Cr^{III/VI}$ redox couples remain unchanged, yet a slightly larger oxidative current was observed in CH_4 at a higher electrochemical potential (E > 2.20 V vs. Hg_2SO_4/Hg) (Figures 2A and S1). As the metal centers have already been at their terminal oxidation states when E > 2.00 V vs. Hg_2SO_4/Hg (vide supra), the larger oxidative currents under 1-bar CH_4 environment suggest additional removal of electrons from metal-bound ligand (Figure 1C) and likely the concurrent CH_4 activation. Here the

magnitude of catalysis-induced oxidative current is presumably limited by the solubility of CH_4 at 1-bar pressure (about 1 mM)[3b] in comparison with the 10-mM concentration of d^0 metals, and the hypothesized mechanism (vide infra) indeed minimizes the differences of oxidative currents in CH_4 and N_2. Despite the technical challenges of cyclic voltammetry in the demanding solvent (Experiments and Methods in SI), our data at least hint that Ti^{IV}, V^{V}, and Cr^{VI} are electrocatalytic towards CH_4, while Ti^{IV} exhibits the lowest anodic

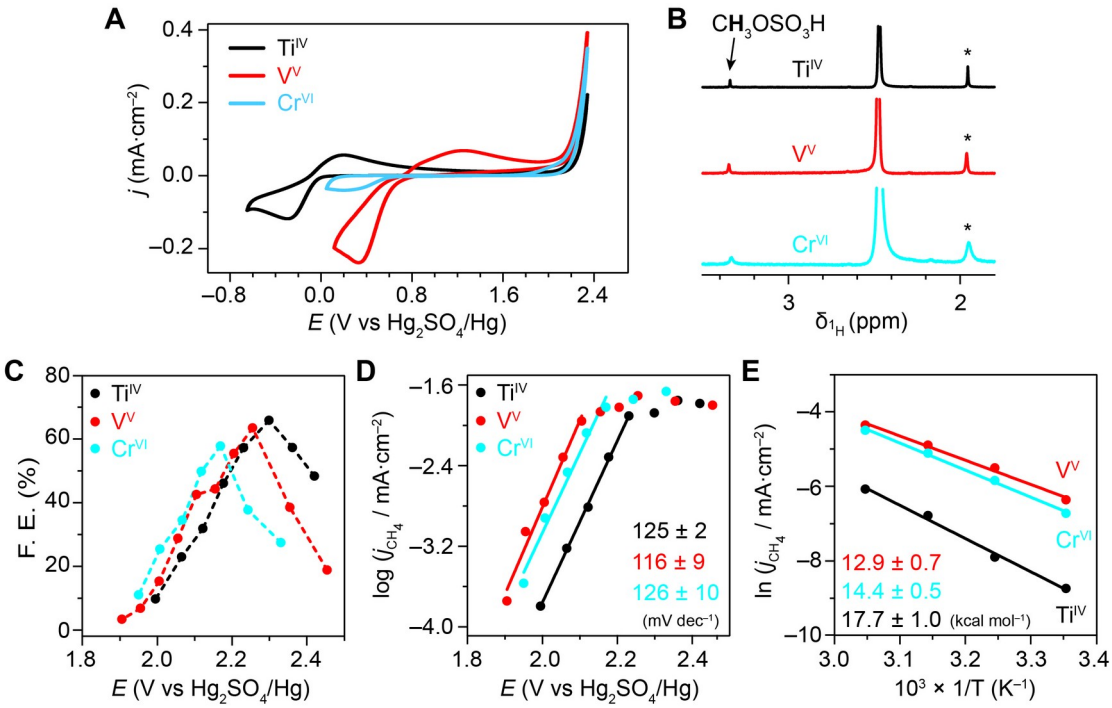

Figure 2. (A) Cyclic voltammograms for Ti^{IV} (black), V^{V} (red), and Cr^{VI} (blue) in 98% H_2SO_4 under 1-bar CH_4. 100 mV/s. (B) ^1H NMR spectra of liquid samples after 6-hr electrolysis with Ti^{IV}, V^{V}, and Cr^{VI} in 98% H_2SO_4 at 2.20 V vs. Hg_2SO_4/Hg. *, internal standard acetic acid. (C) F. E. of CH_4 functionalization with Ti^{IV}, V^{V},[7] and Cr^{VI} in 98% H_2SO_4 versus electrode potential E. (D) log(j_{CH4}) versus E for Ti^{IV}, V^{V},[7] and Cr^{VI} in 98% H_2SO_4 with the fitted Tafel slopes displayed (R^2 > 0.97). (E) ln(j_{CH4}) versus T^{-1} at 2.00 V vs. Hg_2SO_4/Hg for Ti^{IV}, V^{V},[7] and Cr^{VI} in 98% H_2SO_4. The corresponding apparent energies (E_a) are displayed in the corresponding colors (R^2 > 0.99). Unless noted specifically, 25 °C, 10 mM d^0 metals in reagent-grade 98% H_2SO_4, 1-bar CH_4, data recorded from 6-hr bulk electrolysis.

current density hence possibly the slowest kinetics of CH_4 activation.

We observed ambient electrocatalytic functionalization of CH_4 into CH_3OSO_3H for Ti^{IV}, V^{V}, and Cr^{VI} pre-catalysts, all with appreciable reaction selectivities. Bulk electrolysis with 10 mM Ti^{IV}, V^{V}, and Cr^{VI} pre-catalysts in 98% H_2SO_4 were conducted under 1-bar CH_4 at room temperature for 6 hrs on FTO working electrodes (setup shown in Figure S2). Solution electrolytes were analyzed for possible liquid products from CH_4 by ^1H nuclear magnetic resonance (^1H NMR) spectroscopy and detection of gaseous effluents were attempted by on-line gas chromatography (GC) (Experiments and Methods in SI). Among all cases, bulk electrolysis only yielded CH_3OSO_3H as the liquid product, whose chemical shift δ = 3.34 ppm in ^1H NMR was observed (Figure 2B). No other carbon-containing liquid or gaseous products were identified across the spectra of ^1H NMR (Figure S3) and from on-line GC measurement (Figure S4) within our detection limits, consistent with our prior results in the case with V^{V} pre-catalyst.[7] This suggests that solvent oxidation into persulfate and O_2 [10] are the only possible side reactions in the system. After the electrolysis, the ultraviolet-visible (UV-Vis) absorption spectra of the solution remain unchanged (Figure S5), suggesting the minimal change of soluble metal species after electrolysis. No residual metal signals were observed on the FTO electrodes by X-ray photoelectron spectra (XPS) (Figure S6) and the used FTO electrodes themselves were not electrocatalytically active towards CH_4 when they were tested again in neat 98% H_2SO_4 electrolyte under the same condition (E = 2.20 V or 2.26 vs. Hg_2SO_4/Hg). In our prior study in V^{V} pre-catalyst,[7] *operando* X-ray absorption spectroscopy (XAS) spectra at different values of E indicate an intriguing lower oxidation state of V at larger E near the FTO electrode, which could only be explained by a homogenous, diffusion-controlled electrocatalysis with soluble d^1-M-L intermediate. In conjunction with our prior observations,[7] our data suggest minimal heterogenous intermediates at the electrode surface and support a homogeneous molecular electrocatalysis for a two-electron oxidation of CH_4 into CH_3OSO_3H (Figure 1). Electrolysis with 10 mM Ti^{IV}, V^{V}, and Cr^{VI} and pre-added 0.5 mM CH_3OSO_3H in 98% H_2SO_4 under 1-bar N_2 does not show detectable decrease of CH_3OSO_3H concentration (Figure S7). Our prior experiments with V^{V} pre-catalyst demonstrated CH_3OSO_3H concentration up to ~110 mM yielded from electrolysis and the CH_3OSO_3H was electrochemically stable at 1 M concentration.[7] Those results suggest that the product CH_3OSO_3H is sufficiently stable electrochemically and minimal hurdles of accumulating the product at high concentrations for practical applications. When a chemical oxidant $K_2S_2O_8$ was added in lieu of the electrochemical driving force, no detectable products of CH_4 functionalization were observed with the presence of Ti^{IV}, V^{V}, or Cr^{VI} pre-catalysts (Figure S8). This implies that certain unique CH_4-reactive molecular intermediates were created from the pre-catalysts during electrolysis, and such

intermediates are not of peroxy acid or peroxo nature (e.g. $HSO_4^{\bullet}$) since the addition of $K_2S_2O_8$ did not replicate the reactivities. Furthermore, the electrocatalytic selectivity towards CH_3OSO_3H formation, i.e. the Faradaic efficiency (F. E.), was quantified as a function of E (Figure 2C). Under 1-bar CH_4 and room temperature, CH_3OSO_3H formation was observed when E > 2.00 V vs. Hg_2SO_4/Hg for all three transition metals. Optimal F. E. values of 65.8%, 63.5%, and 57.8% were observed at E = 2.30 V, 2.26 V, and 2.17 V vs. Hg_2SO_4/Hg for Ti^{IV}, V^{V}, and Cr^{VI}, respectively (Figure 2C). We note that our ambient setup does not utilize the full potential of those electrocatalytic systems. Such reported values of F. E. are mostly limited by the mass transport of CH_4 due to its limited solubility at 1 bar pressure.[3b] In support of such an argument of mass transport limitation, electrolysis under 11-bar CH_4 led to significant increases of CH_3OSO_3H concentrations and the values of F. E. for all three metals (Figure S9). Notably, a single-pass conversion of ~1% based on CH_4, hence ~1% yield of CH_3OSO_3H as the sole product, was observed in those electrolysis with 11-bar CH_4 (Figure S9). Nonetheless, those ambient F. E. values as a lower bound demonstrate electrocatalysts selectivity towards CH_4 activation. The similar values of maximal F. E. and the corresponding E hint that Ti^{IV}, V^{V}, and Cr^{VI} in a general formalism d^0-M−L all undergo a similar electrocatalytic mechanism for CH_4 functionalization.

Kinetic and mechanistic studies of the electrocatalysis further support a general mechanism among Ti^{IV}, V^{V}, and Cr^{VI} pre-catalysts. The partial current densities of CH_3OSO_3H generation from CH_4 (j_{CH4}) were analyzed as a function of E and temperature (T). When plotting $\log_{10}(j_{CH4})$ against E (Figure 2D), plateaued j_{CH4} of similar values for all three elements were observed at high E values, as the mass transport of CH_4 limits the catalytic turnover (vide supra) and impede a mechanistically relevant investigation. Hence our Tafel analysis were conducted from the linear regions in Figure 2D. Tafel slopes of 125 ± 2, 116 ± 9, and 126 ± 10 mV/dec (R^2 > 0.97) were obtained for Ti^{IV}, V^{V}, and Cr^{VI} pre-catalysts, respectively. The similar values of Tafel slopes and the similar ranges of E despite different chemical nature of those pre-catalysts suggest a common turnover-limiting step (TLS) among the three electrocatalysts. Based on the observed Tafel slopes of about 120 mV/dec, this common TLS is proposed to be the first electron removal from the pre-catalyst d^0-M−L.[11] Because the TLS precedes the step of CH_4 activation, the differences of oxidative currents between CH_4 and N_2 environments may not be significant as in the case observed in Figure 2A and S1. Moreover, plotting $\ln(j_{CH4})$ versus $1/T$ in the linear region of the $\log_{10}(j_{CH4})$−E plot (E = 2.00 V vs. Hg_2SO_4/Hg) yields the apparent activation energy (E_a) of 17.7 ± 1.0, 12.9 ± 0.7, and 14.4 ± 0.5 kcal/mol for Ti^{IV}, V^{V}, and Cr^{VI} pre-catalysts, respectively (R^2 > 0.99, Figure 2E). The low values of E_a are in accordance with the observed room-temperature reactivity of CH_4 functionalization.[12] Consistent with the results of cyclic voltammograms (Figure S1), Ti^{IV} seems to be of lower reactivity based on its more anodic position of linear Tafel region (Figure 2D) as well as its relatively higher value of E_a (Figure 2E). We further conducted experiments to inquire the nature of intermediates during electrocatalysis after the presumed turnover-limiting one-electron removal of pre-catalyst d^0-M−L. When bulk electrolysis was conducted in oleum (20% SO_3) instead of 98% H_2SO_4, methanesulfonic acid (CH_3SO_3H) as a new product was observed in addition to CH_3OSO_3H in the presence of Ti^{IV}, V^{V}, or Cr^{VI} pre-catalysts (Figure S10), and the generation of CH_3SO_3H was significantly suppressed after the co-addition of O_2 along with CH_4 (Figure S11). Since the formation of CH_3SO_3H is generally indicative of the chain propagation between $CH_3\bullet$ radical and SO_3 in oleum and O_2 is considered an effective radical quencher,[3g, 6d] the formed CH_3SO_3H in oleum and the O_2-induced quenching leads us to propose the existence of $CH_3\bullet$ radical during the electrolysis for all three transition metals. We attempted trapping the radical intermediates by quenching the V^{V}-containing electrolyte in liquid N_2 during the electrolysis, yet $CH_3\bullet$ radical was not easy to be detected by electron paramagnetic resonance spectroscopy,[7] likely due to its short lifetime and reactive nature.[3] Nonetheless, while we cannot rule out a pathway of heterolytic CH_4 cleavage during electrolysis, our electrochemical characterizations (Figure 2D and 2E) suggest that Ti^{IV}, V^{V}, or Cr^{VI} pre-catalysts (d^0-M−L) all undergo a turnover-limiting one-electron oxidation prior to ambient CH_4 activation with low activation energies, while leads to the formation of CH_3OSO_3H in 98% H_2SO_4 with $CH_3\bullet$ radical as the possible intermediates as suggested with the observed CH_3SO_3H product in oleum and the O_2-induced quenching effect.

We strive to estimate the TOF values of those pre-catalysts. The TOF values of homogeneous electrocatalysts can be calculated as:[5a, 13]

$$TOF = \left(\frac{j_{CH4}}{nFC_{cat}} \right)^2 \frac{1}{D} \quad (1)$$

Here n = 2 for a two-electron oxidation that yields CH_3OSO_3H, F the Faraday constant, C_{cat} and D the concentration and diffusion coefficient of pre-catalysts, respectively. One uncertainty of such calculation is the diffusion coefficient for Ti^{IV}, V^{V}, and Cr^{VI} pre-catalysts, since not all of their redox behaviors are kinetically fast enough for a Randles-Sevcik analysis (Figure 2A)[14] and no other straightforward alternative methods of determining diffusion coefficient were accessible. Nonetheless, we approximated $D = 2.18\times10^{-7}$ $cm^2\bullet s^{-1}$, which is the reported diffusion coefficient of V^{V} pre-catalysts in 98% H_2SO_4.[7] Such an approximation leads to a relative uncertainty of about 20% in the TOF calculation of pre-catalysts (Experiments and Methods in SI). At 1-bar CH_4, the TOFs for those molecular electrocatalysts were estimated to be 64, 483, and 107 hr^{-1} at E = 2.26 V vs. Hg_2SO_4/Hg for Ti^{IV}, V^{V}, and Cr^{VI} pre-catalysts, respectively. Despite the relative uncertainties, those estimated TOFs are appreciable for ambient CH_4 functionalization in comparison with the literature.[3b, 15]

Our understanding in electrocatalytic mechanism demands more detailed structural information of those pre-catalysts, which are not well illustrated despite their ease of preparation. Our previous work unveils a dimeric structure of the V^{V} pre-catalyst,[7] however the structural details of the Ti^{IV} and Cr^{VI} variants are not available while prior reports suggest monometallic structures.[16] Because we were unable to crystalize the soluble Ti^{IV} and Cr^{VI} pre-catalysts, an effort combining X-ray absorption spectroscopy (XAS) and density functional theory (DFT) calculations were attempted to elucidate the pre-catalysts' structures. We obtained the XAS spectra of Ti atoms for Ti^{IV} pre-catalyst, $TiOSO_4$ (*s*), and metallic Ti foil (Figure S12), as well as the spectra of Cr atoms for Cr^{VI} pre-catalyst, K_2CrO_4 (*s*), and metallic Cr foil (Figure S13). Least-square-regression analysis on X-ray absorption near-edge structure (XANES) for electronic structure and oxidation state of metal centers confirms the d^0 electronic structure of metal centers for Ti^{IV} and Cr^{VI} pre-catalysts (Figures S14 and S15). Extended X-ray absorption fine structure (EXAFS) spectra for the K-edge of Ti and Cr suggest homogeneous molecular pre-catalysts whose coordination environments are different from $TiOSO_4$ (*s*) and K_2CrO_4 (*s*) (Figures S12B and S13B). Additional structural understanding was fetched by structural optimization from DFT calculations and the concurrent structural fitting of the obtained EXAFS spectra (Experiments and Methods in SI).[17] A six-coordinated Ti in Ti^{IV} pre-catalyst was suggested from Ti's pre-edge region in the XANES spectrum after comparing with a library of model compounds (Figure S16).[18] This input leads to a DFT-predicted electroneutral molecule $Ti(SO_4H)_2SO_4$ (Figure 3A) that

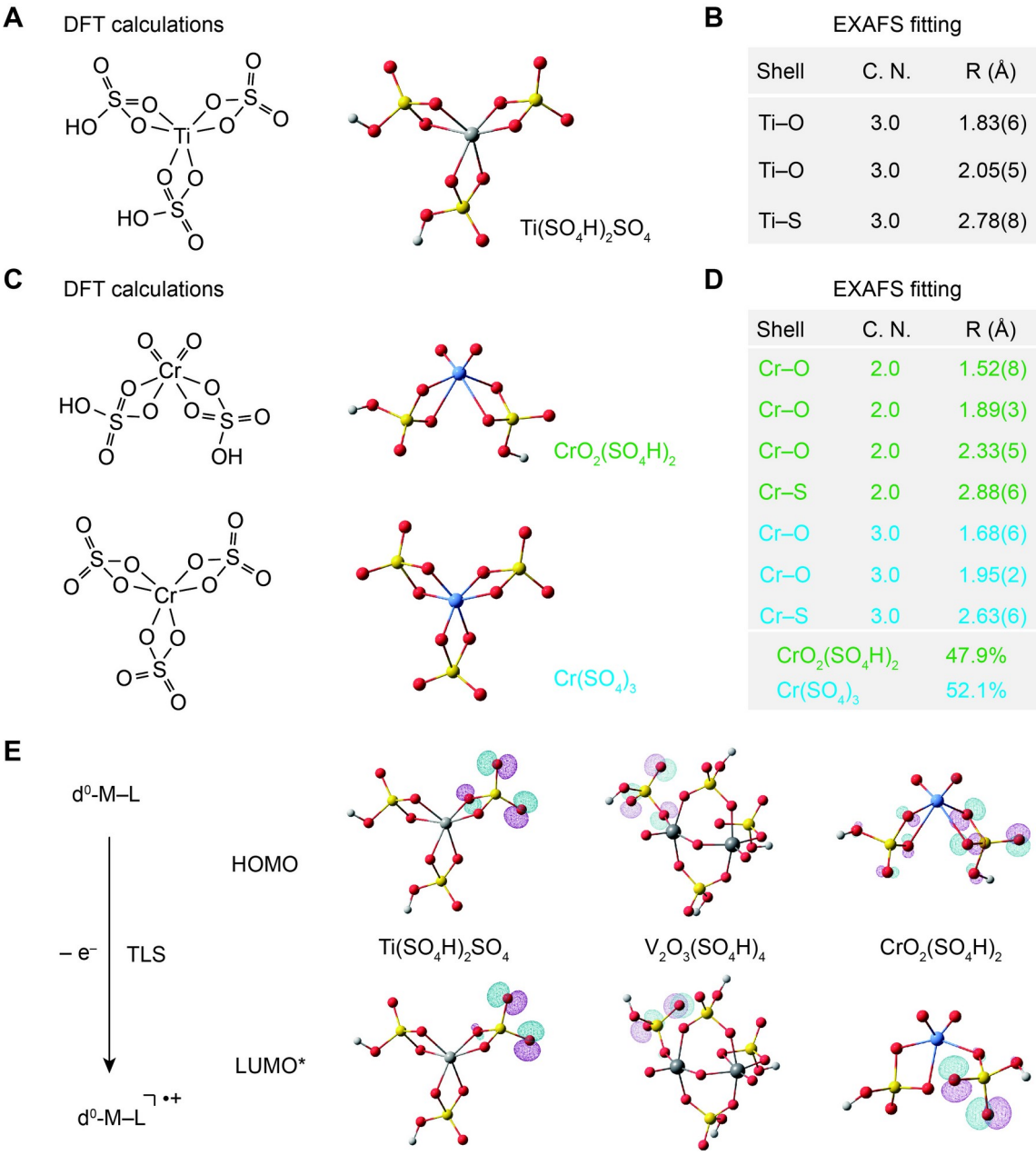

Figure 3. (A, C) The structures of Ti^{IV} (A) and Cr^{VI} (C) pre-catalysts based on DFT calculations. (B, D) The calculated coordination numbers (C. N.) and the distances (R) away from Ti and Cr atoms for Ti^{IV} (B) and Cr^{VI} (D) pre-catalysts based on EXAFS results. (E) The calculated frontier orbitals of pre-catalysts (d^0-M–L) and the ligand-centered cation radicals d^0-M–$L^{\bullet+}$ after the turnover-limiting step (TLS) of one-electron oxidation. HOMO, highest occupied molecular orbital; LUMO*, lowest unoccupied molecular orbital when considering spin-orbital coupling, equivalent to singly occupied molecular orbital (SOMO) in restricted formalism.

yields a satisfactory fitting of the EXAFS spectra only when a monometallic structure was assumed (Figure 3B, Figure S17, and Table S1). Similar procedure was conducted for the Cr^{VI} pre-catalyst. The weak Cr pre-edge feature of Cr^{VI} pre-catalyst (Figure S13A) combined with the simulated XANES results (Figure S18) suggests two six-coordinate candidate structures (Figure 3C) out of the four suggested by DFT calculations (Figure 3C, Figures S19 and S20), and the linear combination fitting (LCF) of the simulated XANES spectra for these two monometallic candidates is satisfactorily consistent with the experimental results (Figure S21). Yet a satisfactory fitting of EXAFS spectra was only achievable by assuming a co-existence of two lowest-energy monometallic species, $CrO_2(SO_4H)_2$ and $Cr(SO_4)_3$, (Figure S22) in a roughly 50:50 ratio (Figure 3D and Table S2). Accordingly, the Cr^{VI} pre-catalyst is considered indeed a mixture of two Cr^{VI} molecules at room temperature.

The structure information and DFT calculations of Ti^{IV}, V^{V}, and Cr^{VI} pre-catalysts (d^0-M−L) offer a reckoning towards a generally applicable mechanism among the investigated systems. Our experimental results suggest that a turnover-limiting one-electron removal from the d^0-M−L pre-catalysts precedes the step of CH_4 activation

with CH_3• as the intermediate. DFT calculations based on our derived structures suggest that such one-electron oxidation will remove one electron from the O 2p orbitals, the highest occupied molecular orbital (HOMO), in the sulfate (Ti^{IV}) or bisulfate (V^{V} and Cr^{VI}) ligands (Figure 3E) and yield a reactive

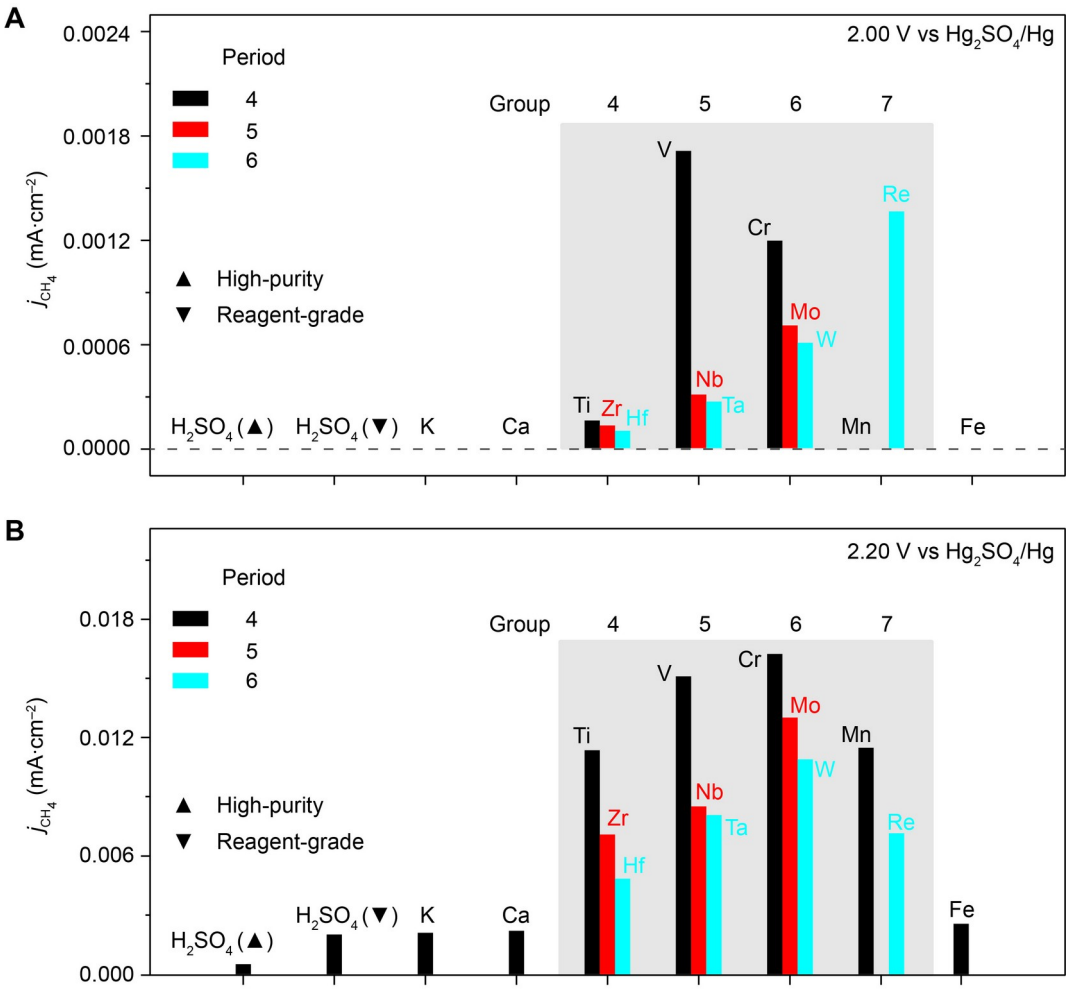

Figure 4. The current density of CH_3OSO_3H generation (j_{CH4}) at E = 2.00 V (A) and 2.20 V (B) vs. Hg_2SO_4/Hg in 98% H_2SO_4. The d^0 early transition metals from Period 4 to 6 in the periodic table are investigated. Common impurities of K^+, Ca^{2+}, and Fe^{2+} were tested for comparison. ▲ & ▼, high-purity (▲) and reagent-grade (▼) 98% H_2SO_4 without added metal species, which contains 0.3 and 5 ppm metal residues, respectively. Scandium (Sc) and technetium (Tc) elements were not studied due to the insolubility of commercially available Sc^{III} compounds and the radioactive property of Tc. Unless noted specifically, 25 °C, 10 mM d^0-M–L in reagent-grade 98% H_2SO_4, 1-bar CH_4, data recorded from 6-hr bulk electrolysis.

cation radical d^0-M−$L^{\bullet+}$ with an empty frontier spin-orbital on the same O 2p orbitals (Figure 3E). In the case of Cr^{VI} mixture, although one-electron removal occurs on the ligands for both $CrO_2(SO_4H)_2$ and $Cr(SO_4)_3$, the calculated ionization energy of $CrO_2(SO_4H)_2$ is lower by 10 kcal/mol than that of $Cr(SO_4)_3$ and $CrO_2(SO_4H)_2$ is considered directly responsible for the observed electrocatalytic activity. The calculated ionization energies of d^0-M−L follow a trend of V^V < Cr^{VI} < Ti^{IV} (Figure S23), which is consistent with our experimentally observed Tafel plots (Figure 2D), the estimated TOF values (vide supra), and the measured apparent activation energies (Figure 2E, see Experiments and Methods in SI). Additional DFT calculations suggest that the d^0-M−$L^{\bullet+}$ first undergoes a fast deprotonation by exchanging proton with solvent, and then a step of CH_4 activation without a significant activation energy barrier (Figures S24, S25, and S26 for Ti, V, and Cr electrocatalysts, respectively). The calculated barrier-less C–H activation is also consistent with the experimental observation that the first one-electron removal from d^0-M–L is the TLS (Figure 2D). The formation of CH_3• and the subsequent radical rebound process[19] is considered viable by DFT calculations and leads to the formation of a d^1-metal intermediate (d^1-M–L) after partial deligandation (Figures S24, S25, and S26). Intermediate d^1-M–L is proposed to regenerate the initial d^0-M–L pre-catalyst via electrochemical oxidation with a smaller energy barrier than that of TLS (Figure 1C, Figures S24, S25, and S26). Despite their difference in molecular structure, a common electrocatalytic mechanism of CH_4 activation is supported by experimental and computational evidence for Ti, V, and Cr electrocatalysts.

A common mechanism among first-row early transition metals motivates us to further expand the set of tested transition metals and confirm their reactivities of CH_4 electrocatalysis in 98% H_2SO_4. We tested early transition metals from Period 4 to Period 6 whose simple salts are isotopically stable and soluble in 98% H_2SO_4. The values of j_{CH4} for CH_3OSO_3H generation from CH_4 at room temperature and 1-bar CH_4 were recorded and two

electrolysis conditions (E = 2.00 V and 2.20 V vs. Hg_2SO_4/Hg) were employed to obtain a more informative picture of the elements' reactivity (Figure 4). Electrolysis results without metal pre-catalysts were also recorded in reagent-grade 98% H_2SO_4, high-purity 98% H_2SO_4, and 98% H_2SO_4 with excessive amount of K, Ca, or Fe as common impurities (Experiments and Methods in SI). Minimal if any impact from the use of Pt counter and pseudo-reference electrodes in our setup were observed from control experiments (Figure 4 and S27). At both E values, electrolysis with the addition of d^0 early transition metals all yielded appreciatable amount of CH_3OSO_3H (Figure 4) that are much higher than any possible impurities. The values of j_{CH4} tend to decrease for heavier elements within the same group from Period 4 to Period 6, while a gradual increase of j_{CH4} values from Group 4 to Group 6 exists. Notwithstanding the cases of unstable Mn^{VII} and Re^{VII} that demands further investigation,[9] our results suggest that the aforementioned electrocatalytic activities towards CH_4 for first-row (Period 4) early transition metals are also observed for the second-row and third-row elements (Period 5 and 6). While more detailed studies are warranted to fully unveil the catalytic mechanism for each element, we disputably postulate that all of those tested early transition metals in the general formalism d^0-M−L follow the same electrocatalytic mechanism given the general similarity in electronic structures and chemical properties among the same groups of early-transition metal elements.

The observed trends of electrocatalytic activities across the periodic table offer additional insights towards the role of metals in the electrochemical generation of CH_4-reactive ligand-based cation radicals (d^0-M–L$^{\bullet+}$). In our proposed mechanism (Figures 1C and 3E), the TLS is the electron removal from the O 2p orbital, whereby the yielded ligand-bound cation radical is responsible for the CH_4 activation. So, what is the role of the d^0 metals beyond being a ligand carrier in the context of electrocatalytic activities? We propose that the electrochemically generated d^0-M–L$^{\bullet+}$ intermediate is partly stabilized by the orbital delocalization between the metal's d orbitals and the radical-bound O 2p orbital.[7] A corollary of this hypothesis is that a smaller energy difference between the metals' d orbital and O 2p one in d^0-M–L$^{\bullet+}$ warrants a more effective orbital delocalization,[20] a more stable d^0-M–L$^{\bullet+}$ once electrochemically generated, and a larger probability of CH_4 activation despite CH_4's limited solubility before the deactivation of d^0-M–L$^{\bullet+}$ due to detrimental side reactions. As the energy differences between metals' 3d (–9.2 ~ –10.7 eV) and O 2p (–15.8 eV) orbitals are appreciably smaller than that for 4d metals (–8.3 ~ –9.1 eV) and even smaller than 5d metals (–6.1 ~ –8.7 eV) (Table S3), the proposed mechanism predicts decreasing CH_4-activating activities when the metal in d^0-M–L$^{\bullet+}$ intermediate changes from Period 4 to Period 6, consistent with our experimental observation (Figure 4). Similarly, as the energy differences between metals' d and O 2p orbitals decreases from Group 4 to Group 6 within the same period (Table S3), CH_4-activating activities are presumed to increase from Group 4 to Group 6, which is satisfactorily observed in our experiments notwithstanding the V-based electrocatalysts at low electrochemical driving forces (Figure 4). The higher-than-expected j_{CH4} values at 2.00 V vs. Hg_2SO_4/Hg for V^V pre-catalyst (Figure 4A) is attributed to the dimeric structure of V^V pre-catalysts,[7] which would offer more energy stabilization for the yielded d^0-M–L$^{\bullet+}$ as evident in the lower calculated ionization energy (Figure S23) and experimentally measured E_a (Figure 2E). Such an oddity of V^V pre-catalyst seems to vanish at a higher E (2.20 V vs. Hg_2SO_4/Hg, Figure 4B), corroborating that the solubility and mass transport of CH_4 (Figure 2D) should also be considered when interpreting j_{CH4} at higher E values. Nonetheless, a general trend of ambient electrocatalytic CH_4 functionalization is tentatively proposed across the periodic table for d^0-M–L electrocatalysts, and the evolution of their reactivities can be satisfactorily explained in the first-order approximation by our working hypothesis regarding the stability of electrochemically generated d^0-M–L$^{\bullet+}$ intermediate. Although V^V pre-catalyst's performance remains the best among the discovered electrocatalysts, three lessons could be learned here: (1) it seems viable to employ metal-bound bisulfate as a redox-active ligand with electro-generated cation radicals to conduct electrocatalytic CH_4 activation, given the universal reactivities discovered in this work; (2) the metal centers in the pre-catalyst is proposed to stabilize electro-generated cation radicals d^0-M–L$^{\bullet+}$ by the orbital delocalization between metals' d orbitals and O atom's p orbitals in the bisulfate ligand, thanks to the reactivity trend of different metals that correlates with the metals' d orbital energies; (3) In addition to metals' d orbital energies, dimerization offers further orbital delocalization that stabilizes the electro-generated d^0-M–L$^{\bullet+}$, leading to more active CH_4 electrocatalysis. These working hypotheses hint that large clusters of early transition metal-oxo species with suitable d orbital energy overlap, which could be nanoscale materials, are promising candidates for advanced electrocatalysts for ambient CH_4 functionalization.

Conclusion

In summary, we report a new class of ambient electrocatalytic CH_4 functionalization generally applicable for d^0 early transition metals. With first-row early metals of Ti, V, and Cr as the model systems, we found a common electrocatalytic mechanism towards those transition metals in 98% H_2SO_4 that explains the relative reactivity trend across the periodic table. While d^0 early transition metals have not been frequently considered for their applications in electrochemical catalysis, our experimental results and the derived design principles suggest ample opportunities for the development of advanced electrocatalysts for CH_4 activation. Additional mechanistic studies for each of the reported elements are needed not only to fully appreciate the mechanism but also to further examine

our working hypothesis. The concept of electrochemically generating reactive O-based radicals for C-H activation will guide future design of electrocatalysis for light alkanes and other organic substrates. The experimentally determined low activation energy, high TOF and Faradaic efficiency are encouraging towards an ambient transformation of natural gas into liquid fuels or commodity chemicals at the flaring or emission locations with minimal infrastructure reliance.

Acknowledgements

H.M.C. acknowledges the Ministry of Science and Technology, Taiwan (Contracts No. MOST 109-2628-M-002-001-RSP and 109-2926-I-002-512). A.N.A. acknowledges the NSF Career Award (CHE-1351968) and the UCLA-IDRE cluster Hoffman2 and CSM HPC clusters for computational resources. C.L. acknowledges the NSF Award (CHE-1955836), startup fund from the University of California, Los Angeles and the financial support of the Jeffery and Helo Zink Endowed Professional Development Term Chair.

Conflict of interest

The authors declare no conflict of interest.

Keywords: electrocatalysis • methane functionalization • early transition metals • d^0 electronic structure • ambient conditions

[1] a) E. McFarland, *Science* **2012**, *338*, 340–342; b) F. Schüth, *Science* **2019**, *363*, 1282–1283.

[2] J. Rostrup-Nielsen, L. J. Christiansen, *Concepts in Syngas Manufacture, Vol. 10 of Catalytic Science Series*, Imperial College Press, London, **2011**.

[3] a) A. E. Shilov, G. B. Shul'pin, *Chem. Rev.* **1997**, *97*, 2879–2932; b) N. J. Gunsalus, A. Koppaka, S. H. Park, S. M. Bischof, B. G. Hashiguchi, R. A. Periana, *Chem. Rev.* **2017**, *117*, 8521–8573; c) R. A. Periana, D. J. Taube, E. R. Evitt, D. G. Loffler, P. R. Wentrcek, G. Voss, T. Masuda, *Science* **1993**, *259*, 340–343; d) R. A. Periana, D. J. Taube, S. Gamble, H. Taube, T. Satoh, H. Fujii, *Science* **1998**, *280*, 560–564; e) T. Zimmermann, M. Soorholtz, M. Bilke, F. Schuth, *J. Am. Chem. Soc.* **2016**, *138*, 12395–12400; f) S. Mukhopadhyay, A. T. Bell, *Angew. Chem. Int. Ed.* **2003**, *42*, 2990–2993; g) N. Basickes, T. E. Hogan, A. Sen, *J. Am. Chem. Soc.* **1996**, *118*, 13111–13112; h) G. V. Nizova, G. SussFink, G. B. Shulpin, *Chem. Commun.* **1997**, 397–398; i) J. A. Labinger, J. E. Bercaw, *Nature* **2002**, *417*, 507–514; j) C. Díaz-Urrutia, T. Ott, *Science* **2019**, *363*, 1326–1329; k) X. G. Meng, X. J. Cui, N. P. Rajan, L. Yu, D. H. Deng, X. H. Bao, *Chem* **2019**, *5*, 2296–2325; l) G. A. Olah, *Acc. Chem. Res.* **1987**, *20*, 422–428; m) R. A. Periana, O. Mironov, D. Taube, G. Bhalla, C. J. Jones, *Science* **2003**, *301*, 814–818.

[4] a) S. Nitopi, E. Bertheussen, S. B. Scott, X. Y. Liu, A. K. Engstfeld, S. Horch, B. Seger, I. E. L. Stephens, K. Chan, C. Hahn, J. K. Norskov, T. F. Jaramillo, I. Chorkendorff, *Chem. Rev.* **2019**, *119*, 7610–7672; b) J. Deng, J. A. Iniguez, C. Liu, *Joule* **2018**, *2*, 846–856.

[5] a) J. M. Savéant, *Elements of molecular and biomolecular electrochemistry. An electrochemical approach to electron transfer chemistry*, Wiley, New Jersey, **2006**; b) N. Sauermann, T. H. Meyer, Y. A. Qiu, L. Ackermann, *ACS Catal.* **2018**, *8*, 7086–7103.

[6] a) M. E. O'Reilly, R. S. Kim, S. Oh, Y. Surendranath, *ACS Cent. Sci.* **2017**, *3*, 1174–1179; b) R. S. Kim, Y. Surendranath, *ACS Cent. Sci.* **2019**, *5*, 1179–1186; c) R. S. Kim, E. C. Wegener, M. C. Yang, M. E. O'Reilly, S. Oh, C. H. Hendon, J. T. Miller, Y. Surendranath, *J. Am. Chem. Soc.* **2020**, *142*, 20631–20639; d) R. S. Kim, A. Nazemi, T. R. Cundari, Y. Surendranath, *ACS Catal.* **2020**, *10*, 14782–14792.

[7] J. Deng, S. C. Lin, J. Fuller, J. A. Iniguez, D. L. Xiang, D. Yang, G. R. Chan, H. M. Chen, A. N. Alexandrova, C. Liu, *Nat. Commun.* **2020**, *11*, 3686.

[8] a) N. Fatouros, D. Krulic, N. Larabi, *J. Electroanal. Chem.* **2004**, *568*, 55–64; b) C. Madic, G. M. Begun, R. L. Hahn, J. P. Launay, W. E. Thiessen, *Inorg. Chem.* **1984**, *23*, 469–476; c) A. F. Diaz, D. Schermer, *J. Electrochem. Soc.* **1985**, *132*, 2571–2575.

[9] N. N. Greenwood, A. Earnshaw, *Chemistry of the elements, 2nd Edition*, Butterworth-Heinemann, **1997**.

[10] a) J. Zhu, K. K. Hii, K. Hellgardt, *ACS Sustain. Chem. Eng.* **2016**, *4*, 2027–2036; b) I. M. Kolthoff, I. K. Miller, *J. Am. Chem. Soc.* **1951**, *73*, 3055–3059.

[11] Gileadi E., *Physical electrochemistry: fundamentals, techniques and applications*, Wiley-VCH, **2011**.

[12] I. Levine, *Physical chemistry*, McGraw-Hill Higher Education, **2009**.

[13] C. Costentin, S. Drouet, M. Robert, J. M. Saveant, *J. Am. Chem. Soc.* **2012**, *134*, 11235–11242.

[14] P. Zanello, *Inorganic electrochemistry: theory, practice and application*, Royal Society of Chemistry, London, **2003**.

[15] B. L. Conley, W. J. Tenn, K. J. H. Young, S. K. Ganesh, S. K. Meier, V. R. Ziatdinov, O. Mironov, J. Oxgaard, J. Gonzales, W. A. Goddard, R. A. Periana, *J. Mol. Cat. A-Chem.* **2006**, *251*, 8–23.

[16] a) Y. A. Lisitsyn, N. V. Busygina, Y. I. Zyavkina, V. G. Shtyrlin, *Russ. J. Electrochem.* **2010**, *46*, 512–523; b) R. J. Gillespie, R. Kapoor, *Can. J. Chem.* **1987**, *65*, 2665–2669.

[17] G. Bunker, *Introduction to XAFS: a practical guide to X-ray absorption fine structure spectroscopy*, Cambridge University Press, Cambridge, **2010**.

[18] F. Farges, G. E. Brown, J. J. Rehr, *Phys. Rev. B* **1997**, *56*, 1809–1819.

[19] X. Y. Huang, J. T. Groves, *J. Biol. Inorg. Chem.* **2017**, *22*, 185–207.

[20] S. Inagaki, *Orbitals in chemistry*, Springer, **2010**.

Entry for the Table of Contents

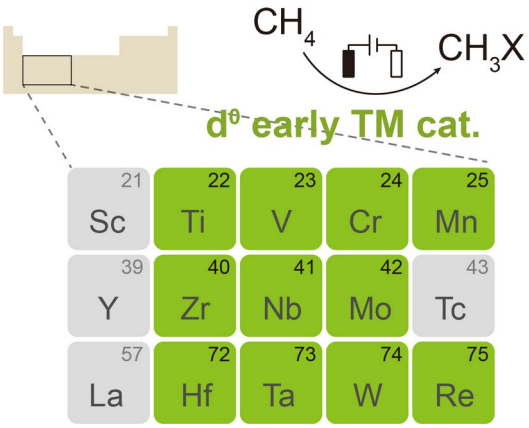

This study reports a general class of electrocatalysts covering the majority of early transition metals for ambient methane functionalization. The broad applicability of this discovery offers fundamental insights and new opportunities for natural gas utilization.